Fatigue performance of composite-steel injected connectors at room and elevated temperatures

Christoforidou, Angeliki; Pavlovic, Marko

DOI
10.1016/j.engstruct.2024.118421

Publication date
2024

Document Version
Final published version
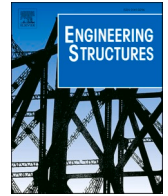
Published in
Engineering Structures

Important note
To cite this publication, please use the final published version (if applicable).
Please check the document version above.

Fatigue performance of composite-steel injected connectors at room and elevated temperatures

Angeliki Christoforidou , Marko Pavlovic [*]

TU Delft, Steel and Composite Structures, Delft, the Netherlands

ABSTRACT

The integration of Glass Fibre-Polymer composite (a.k.a. GFRP) deck panels in bridge infrastructure is hindered by lacking a robust connection technology. A promising bolted connection, utilising injected steel reinforced resin (iSRR) material, has demonstrated lower creep deformation and sustained significantly more shear load cycles than conventional bolts. Nonetheless, the production and testing conditions in all prior experimental campaigns followed idealized lab set-ups. This study bridges the gap between laboratory conditions and the challenges arising during connector's fabrication under representative conditions, coupled with cyclic load testing at room and elevated temperatures. The iSRR connectors design is modified and tested in actual composite sandwich web core panels, revealing excellent fatigue performance. The statistical analysis yielded F-N curves for shear performance of the connectors that can be used in the design. The slopes of the F-N curves of − 6.6 and − 5.8 were found at room and elevated temperatures, respectively. Finally, with post-cyclic static tests displaying significant connectors' residual stiffness, resistance, and ductility, the research provides a step forward in enabling the integration of glass fibre composite deck in infrastructure.

1. Introduction

A significant proportion of extant bridges in Europe were designed and erected during the post-World War II epoch. Evidently, the engineering standards of this era did not adequately account for contemporary traffic intensity and vehicular loading capacities. As an example, the tandem system and the uniformly distributed loads based on Load Model 1 from Eurocode EN1992–1 exhibit a 100 % and 125 % increase, respectively, when juxtaposed with the design standard established in 1963 used in the Netherlands [1,2]. Subsequent inspection and reassessment of these structures have not surprisingly revealed their fatigue and corrosion-related complications [3].

To counter these challenges, a range of novel materials including Ultra-High Performance Concrete (UHPC) [4,5], Steel Fibre Reinforced Concrete (SFRC) [6], Engineered Cementitious Composites (ECC) [7], Fibre Reinforced Polymer (FRP) panels [8,9], and other advanced composites are increasingly considered for future bridge rehabilitation and construction. A critical aspect of these solutions is the shear connector, which significantly influences the structural performance and stiffness of the beam [10]. Demountable shear connectors are extensively researched due to their pivotal role in enhancing modularity and easing future maintenance. Solutions such as bolts with embedded single or double nuts or couplers [11–14], high-tension friction-grip bolts [15], injection bolts [16], blind bolts [17,18], and demountable headed stud shear connectors [19] have been developed in the pursuit of more sustainable and adaptable infrastructure.

Due to a noticeable gap in the literature and their high potential for addressing the prevalent issues of corrosion and fatigue in bridge structures, this paper will focus on the development of a demountable shear connector for FRP decks. The lightweight nature of these decks alleviates the necessity for future reinforcement of the well-maintained steel substructures, which will remain unrenovated. Moreover, composites' durability offers protection to the steel girders against extreme environmental conditions, while their high strength-to-weight ratio and customizable elements exhibit superior fatigue resistance [20]. Nevertheless, the restricted availability of a generic and practicable connection technology has hindered its widespread implementation.

Currently, the most prevalent solutions for structural connections between composite and steel are bolted and bonded solutions. Bolted connections suffer from slip due to bolt-to-hole clearances and therefore have insufficient initial stiffness [21]. Their relatively poor fatigue and creep behaviour due to localized bearing stresses around the hole in the

(a) Global view

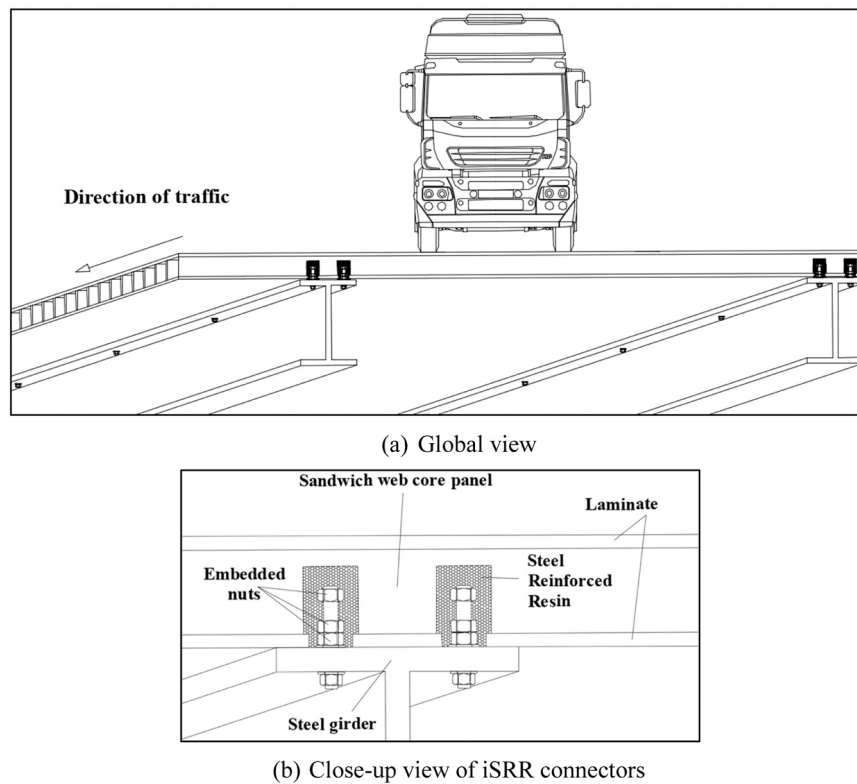(b) Close-up view of iSRR connectors

Fig. 1. Cross section of a bridge with iSRR bolted connections between composite deck panel and steel girder.

composite material has limited their application [22]. Bonded connections can be a viable solution but can have a very unpredictable brittle failure and their susceptibility to environmental influences is insufficiently known [23].

A less frequently employed approach involves the use of injection materials to embed mechanical connectors within composite structural elements. Presently, polymer resins or cementitious grouts serve this purpose, albeit with certain limitations. Shear stud connections embedded in cement-based grout have exhibited satisfactory performance in static and fatigue tests [24]. However, their effectiveness is contingent upon the degree of confinement within the composite member and the relatively low tensile strength of the grout, necessitating the employment of local spiral reinforcement around connectors. Moreover, the creep behaviour and environmental durability of grout-injected connections have yet to be thoroughly investigated.

Injection bolts could be beneficial in terms of execution efficiency, demountability and have shown promising fatigue behaviour at low frequencies (0.04 to 3.3 Hz) [25]. However, as the frequency increases, the fatigue performance of this type of bolts significantly diminishes [25, 26]. It has also been argued that the small diameter of the hole in the composite leads to generation of high bearing stresses that deteriorates the short- and long-term performance of the injected bolt connector [26]. In light of the aforementioned, a novel type of connector is developed that uses normal bolts (or rods) which are surrounded by resin reinforced by steel shot. This relatively new type of injection material, invented by Nijgh [27], is poured into a large and almost cylindrical hole inside the composite deck that encloses the mechanical connector as Fig. 1 indicates. Consequently, the injected material in this application is encircled by the composite bottom facing and the foam of the sandwich web core panel.

Preliminary research demonstrated the applicability of injected steel-reinforced resin connections, from now on referred to as iSRR, as a composite-to-steel connector in infrastructure. From static push-out tests, the iSRR connector with an M20 bolt diameter illustrated a comparable stiffness and shear resistance with the steel-concrete hybrid

structures connected with the same bolts' diameter [28]. Tests on a glass fibre composite-to-steel single-lap joint (SLJ) configuration revealed that iSRR connectors can yield a 42 % lower creep deformation compared to injected bolts with conventional resin [26]. Moreover, these joints sustained 290 and 100 times more fully reversed shear load cycles at the same load regime compared to blind and conventionally injected bolts, respectively [26,29].

The iSRR connector, although it has been subjected to both short-term and long-term loading, has not been previously exposed to temperatures exceeding typical room temperatures (20 - 25 °C). Furthermore, its fabrication and testing have consistently occurred under the favourable conditions of a laboratory setting. This involved working with perfectly flat panels that facilitated the direct contact between the composite facing and the steel plate, and all tests were executed at ambient temperature with no examination of potential influences from elevated temperatures.

Research on both mechanically connected and adhesively bonded joints, as evidenced in current literature, underscores the significant influence of thermal conditions. For instance, single- or double-bolted pultruded composite or glass fibre composite profiles exhibited considerable strength reductions and alterations in failure modes when subjected to high temperatures and static loading [30–32]. This trend was also observed in [33] and [34] works on adhesively bonded joints, which highlighted the critical role of cyclic creep in fatigue failure, and the potential for temperature and joint geometry to accelerate failure in specific configurations under cyclic loading. These findings serve to emphasize the necessity of exploring the effects of temperature on the fatigue and creep behaviour of such connections.

In response to these findings, this paper seeks to bridge the gap between the idealized laboratory-produced iSRR connector and those manufactured under more representative scenarios, subjected to realistic environmental and loading conditions. As such, several modifications to the iSRR connector's design are proposed and subsequently tested under cyclic and post-cyclic static loading conditions. The experiments are conducted at both room and elevated temperatures, and a
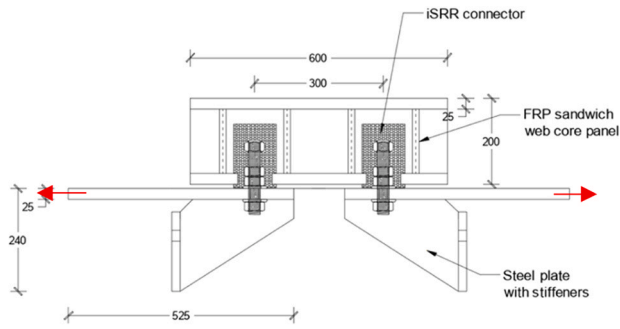
(a) detailed view of configuration (red arrows indicate loading direction)
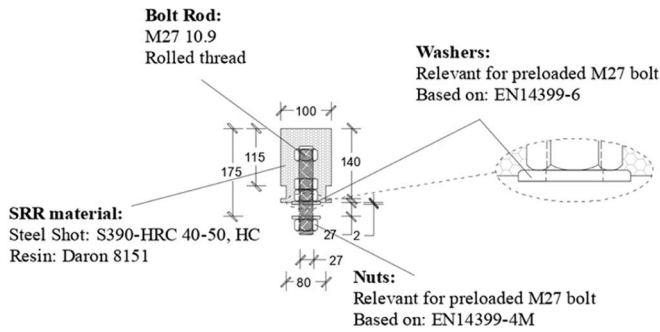
(b) details of the connector

Fig. 2. iSRR connectors in composite-steel single-lap shear joint specimens (dimensions in mm).

Table 1
Stacking sequence of laminates of GFRP deck.

Facings	$[45/-45/45/-45/45/-45/0/90/45/-45/90_3/0/90/45/-45/90_3/0/90/45/-45/90_3/0/90/45/-45/90_3/0/90/45/-45]$
Web	$[-45/45/-45/45/-45/45/90/0/-45/45/-45/45/-45/45]$

Table 2
Material indexes for every utilised component.

Component	Mechanical properties[1]
UD laminate	$E_1 = 31450$ MPa, $E_2 = E_3 = 8459$ MPa, $G_{12} = G_{13} = 4838$ MPa, $G_{23} = 3021$ MPa
	$\nu_{12} = \nu_{13} = 0.272$, $\nu_{23} = 0.4$, $\rho = 1873$ kg/m³
Foam	$E = 2.1$ MPa, $\nu = 0.3$, $\rho = 32$ kg/m³
Steel shot	S390, HRC 40-50, $\rho = 7400$ kg/m³
Resin	$\eta = 150 - 220$ [mPa.s], $E = 3530$ MPa, $T_g = 135$ °C
SRR[37]	$E_t = 16181$ MPa, $f_t = 10$ MPa, $\nu = 0.13$ and $\rho = 4955$ kg/m³
Bolt rod	Grade 10.9, $E = 210000$ MPa, $\nu = 0.3$, S355
Nuts	Grade 10.9, $E = 210000$ MPa, $\nu = 0.3$, S355
Washers	Grade 10.9, $E = 210000$ MPa, $\nu = 0.3$, S355

Note: 1 - E = Young's modulus, G = Shear modulus, ρ = density, S390 = Size of steel shot, HRC = Hardness, Tg = Glass transition temperature under full post-curing, η = viscosity, f_t = Tensile strength, ν = Poisson's ratio

characterisation of the fatigue and static performance of the joint is provided. Finally, this research delves into how the connector's performance and the onset of damage vary across different temperature conditions.
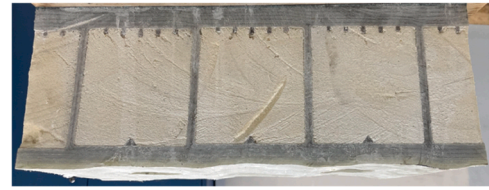

Fig. 3. Glass fibre composite sandwich web core panel used for testing – Realistic bottom facing.

2. Materials and specimens

2.1. Details of specimens

Experiments are conducted utilizing segments from a vacuum-infused glass fibre composite sandwich web-core panel and two steel end-details representing the flanges of steel girders, as shown in Fig. 2 (a). Initially, a long deck panel was vacuum infused by FiberCore using an upside-down approach to ensure that the top side of the deck, which would be on the fixed mold, provides a smooth riding surface. This process leaves the bottom side of the deck, facing the vacuum bag, with a non-smooth surface. The stacking sequence, detailed in Table 1, involves first wrapping the PU foam cores and then adding Z-layers and additional UD plies to create a sandwich panel deck with integrated webs. This fabrication process mirrors the actual practice used in FRP bridge deck construction to ensure consistency and to study the functionality of the iSRR connector at elevated temperatures under a realistic heat transfer.
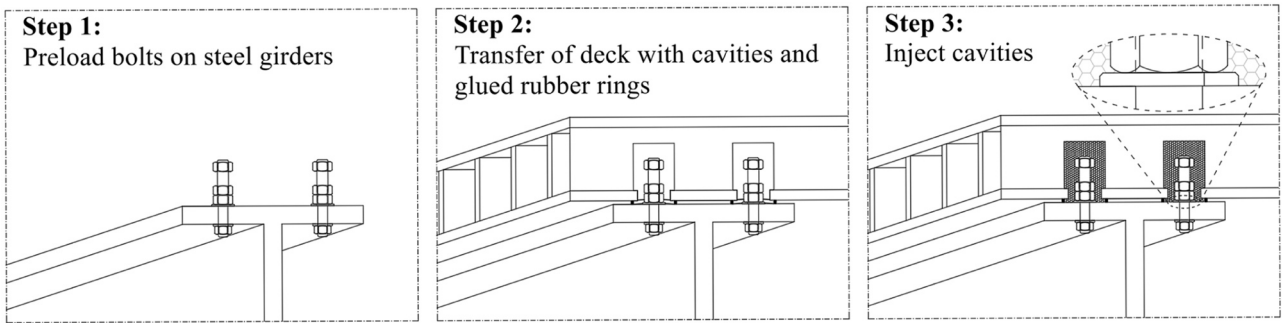
The long deck is subsequently cut into smaller composite panels measuring 600×300×200 mm, with the integrated webs positioned perpendicularly to the loading direction. This orientation is chosen as it has been shown to result in more adverse cyclic degradation, evidenced by increased displacement range accumulation [35].

The iSRR connector is assembled using 10.9 bolt rods of M27 diameter, embedded nuts, and a gap filled with SRR material. Stiffeners are added to the steel plates to increase flexural rigidity and reduce eccentricity of the SLJ setup. This configuration is proven that accurately depicts iSRR connectors' fatigue life based on bending moment analyses in [36]. Every component used in this experimental campaign with their corresponding material indexes are listed in Table 2.
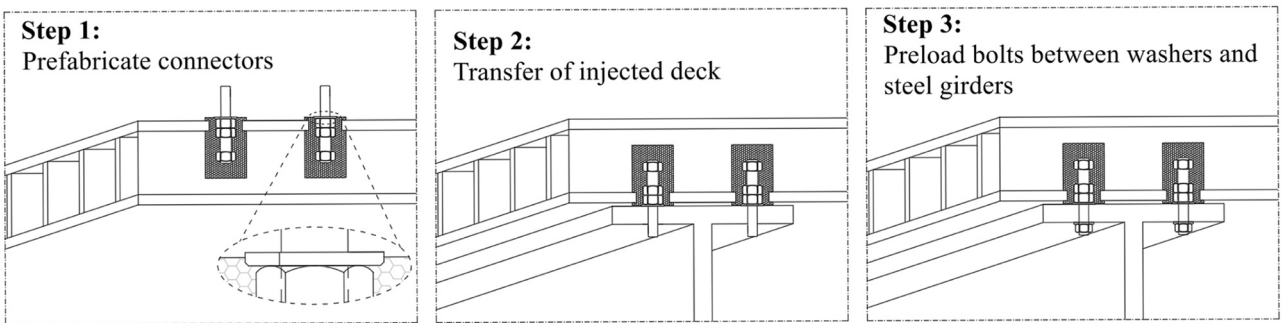
This paper introduces two significant modifications to the iSRR connector design. First, in recognition of the non-flat bottom facing of the composite deck, as shown in Fig. 3, and the non-flat top surface of the steel girder, rubber rings of 8 mm thickness and 100 mm diameter are added around the holes in the composite facing for controlled injection.

Additionally, the fabrication process of iSRR connectors can be conducted either in a factory setting or directly on-site as illustrated in Fig. 4. When fabricated on-site, the bolts are first preloaded into the steel girders. Subsequently, the GFRP deck with its pre-drilled cavities is placed over the steel girders, and the cavities are injected from the top. This method ensures that the preloading of the bolts is completed before the resin injection, preventing any loss of preload during this phase. As a result, the SRR material can safely fill up to the full height of the cavities, encapsulating the entire assembly.

Conversely, in a prefabrication setting, it is crucial to prevent the SRR material from making direct contact with the steel girders. Therefore, as depicted in Fig. 4 (b), the total height of the SRR material is adjusted so that its surface is lower than the top surface of the washer. This separation ensures that the preloading assembly is comprised solely of metallic components without the inclusion of polymeric materials. Thus, effective preload of the bolt throughout the connector's service life is maintained. This adjustment facilitates the prefabrication of the connectors and ensures slip resistance and substantial hybrid interaction between the composite deck and steel substructure.

Step 1:
Preload bolts on steel girders

Step 2:
Transfer of deck with cavities and glued rubber rings

Step 3:
Inject cavities

(a) On-site fabrication of iSRR connectors

Step 1:
Prefabricate connectors

Step 2:
Transfer of injected deck

Step 3:
Preload bolts between washers and steel girders

(b) Prefabricated iSRR connectors

Fig. 4. Procedures for producing iSRR connectors.
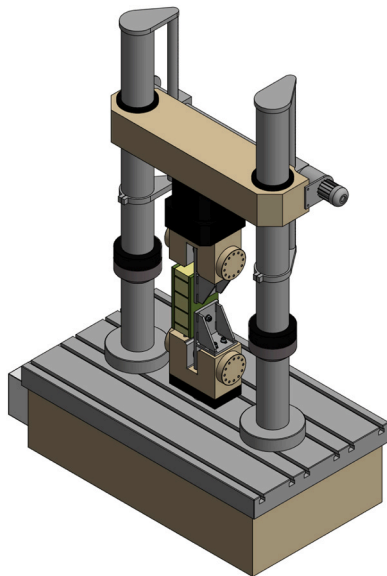
Fig. 5. Test setup of cyclic and static tests under ambient temperature.

Fig. 6. Test setup of cyclic and static tests under elevated temperature; (a) schematic view of the chamber, (b) open chamber.

Regardless of the fabrication method, whether prefabricated with a specific height adjustment or directly filled on-site, the retention of the desired preloading and integrity of the connection throughout its lifetime is ensured.

2.2. Set up configuration

The comprehensive experimental setup is depicted in Fig. 4. All cyclic and static tests are executed in an Instron dual-column testing equipment with a load cell capacity of 600 kN. Part of the steel end detail is clamped in the hydraulic jaws, whilst their horizontal elements are fastened to the upper and (movable) lower cross heads. To control the temperature at 55 °C, a custom-built chamber is constructed using insulating panels. The dimensions of the panels and a schematic representation of the chamber, along with a photograph illustrating its appearance, are provided in Fig. 5. Air circulation within the test chamber is facilitated by a fan and a motor. To ensure that the temperature remained constant at the specified level, two temperature

Table 3
Matrix with experimental parameters.

Loading Condition	Load level	Environmental condition	No. of connectors
Cyclic	±40 kN	Ambient temperature	4
Cyclic	±40 kN	Elevated temperature	4
Cyclic	±60 kN	Ambient temperature	4
Cyclic	±60 kN	Elevated temperature	4
Cyclic	±80 kN	Ambient temperature	4
Cyclic	±80 kN	Elevated temperature	4
Static	Monotonic	Ambient temperature	12
Static	Monotonic	Elevated temperature	12

sensors were positioned adjacent to the steel stiffeners, as illustrated in Fig. 6 (b). The sensors' tips were specifically placed near the two bolt regions.

2.3. Joint specimens and instrumentation

A total of 12 specimens, comprising 24 connectors, are prepared and tested using the following naming convention: X-YY-ZZ-D-C. The first letter (X) indicates the type of loading, which can be either cyclic or static loading once the fatigue test is terminated. The set of letters YY refers to the maximum load applied during the cyclic test. The last group of letters (ZZ) indicates the exposed temperature, which can either be room temperature (RT) or elevated temperature of 55 °C denoted as ET. The digit (D) can either be 1 or 2, referring to the number of specimens tested with the same parameters X, YY, ZZ. Lastly, due to the fact that there are two connectors (C) in one tested panel, the last letter (C) can either be T or B, depending on the location of the joint; T for the top and B for the bottom. The various experimental parameters considered are presented in Table 3.

The temperature is continuously monitored using temperature sensors and thermocouples for the chamber and the connectors, respectively. The tip of the temperature sensors is located close to the bolt region adjacent to the steel stiffener. In 9 of the joints (three tested at room temperature and all the specimens tested at 55 °C), 2 thermocouples are installed inside the SRR piece, with one thermocouple near the rod and the other near the foam, as shown in Fig. 7. The purpose of using the thermocouples is to track the temperature rise for the specimens tested inside the temperature chamber. They are also used for half

Fig. 7. Location of thermocouples; next to bolt's head (nut) and in foam.
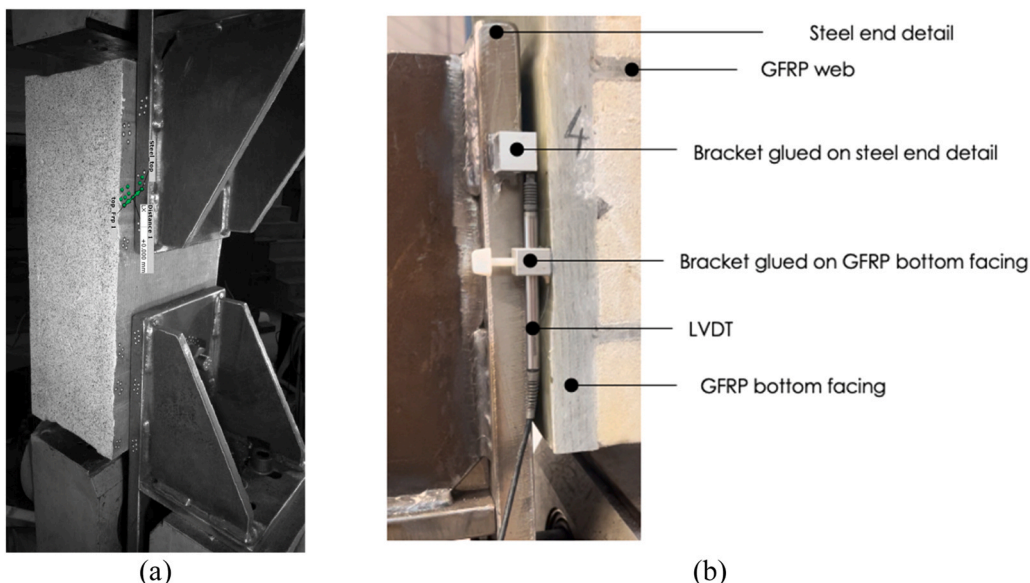

(a)   (b)

Fig. 8. Instrumentation of specimens for measuring FRP-steel relative displacement; (a) photo taken from 3D DIC system, (b) close up of one LVDT.

Table 4

Instrumentation applied in each specimen.

Loading	Temp	No. of test	Cyclic instrumentation	Static[1] instrumentation
Low	25 °C	1	4 LVDTs	2 systems of 3D DIC
(± 40 kN)	25 °C	1	4 LVDTs + 4 Thermocouples	4 LVDTs + 4 Thermocouples
	55 °C	2	4 LVDTs + 4 Thermocouples	4 LVDTs + 4 Thermocouples
Medium	25 °C	1	4 LVDTs	2 systems of 3D DIC
(± 60 kN)	25 °C	1	4 LVDTs + 4 Thermocouples	4 LVDTs + 4 Thermocouples
	55 °C	2	4 LVDTs + 4 Thermocouples	4 LVDTs + 4 Thermocouples
High	25 °C	1	4 LVDTs	2 systems of 3D DIC
(± 80 kN)	25 °C	1	4 LVDTs + 4 Thermocouples	4 LVDTs + 4 Thermocouples
	55 °C	2	4 LVDTs + 4 Thermocouples	4 LVDTs + 4 Thermocouples

Note: 1 - static after fatigue loading

Table 5

Cycles of loading depending on load level and temperature.

Cyclic loading	Temperature	Stop criterion
Low (± 40 kN)	25 °C	Cycles exceeded 2500000
	55 °C	Cycles exceeded 2000000
Medium (± 60 kN)	25 °C	Displacement range increase of 0.3 mm or cycles exceeded 1500000
	55 °C	Displacement range increase of 0.3 mm or cycles exceeded 1000000
High (± 80 kN)	25 °C	Displacement range increase of 0.3 mm
	55 °C	Displacement range increase of 0.3 mm

of the experiments performed at ambient temperature to monitor the temperature increase due to cyclic loading. In four of the joints, the temperatures are tracked during the resin curing process to understand the resin's reactivity and monitor its gel time, i.e., when the temperature of the resin increases from 25 °C to 35 °C. The gel point of the resin is particularly important in this application since, after this point, the resin crystallizes, and no further injection can be performed.

For the static tests, three out of twelve experiments are performed using a pair of 3D digital image correlation (DIC) systems from GOM Aramis, featuring 800 mm adjustable base, 12 mpx cameras, and 50 mm lenses (see Fig. 8 (a)). This setup ensures comprehensive monitoring of possible composite failure on both sides of the panel or out-of-plane motions. For the remaining static experiments, the independent connector slip behaviour of the two connectors in one specimen is determined by placing a pair of linear variable differential transducers (LVDTs) on both sides of each connector, as shown in Fig. 8 (b). This is particularly necessary for the tests at 55 °C since the DIC systems cannot be used as the chamber encloses the specimen. Due to the 10 mm displacement limit of the LVDT, once the displacement capacity is reached, the LVDTs are readjusted, and the test resumes. This action has no effect on the temperatures inside the iSRR connector, as no drop in the temperatures was observed. Heating the chamber and maintaining the elevated temperature has no appreciable effect on the LVDTs' performance. For the cyclic experiments, four LVDTs are placed to obtain the additional displacement range increase of each connector. Table 4 presents all the test set-ups including their instrumentation.

3. Test procedure

3.1. Cyclic loading regime

Long-term loading is applied to the specimens at three designated levels: low, medium, and high. These levels are defined by maximum loads of 40, 60, and 80 kN, respectively, corresponding to

approximately 15 %, 22.5 %, and 30 % of their ultimate static shear resistance. The selection of these load levels stems from preliminary structural analyses of steel girders connected with fibre-polymer composite decks [38]. In these analyses, a load range of 62 kN is identified as the upper limit for the maximum cyclic forces exerted on connectors situated at the deck's edge. A fully reversed load ratio (R = −1) is employed, based on its expected contribution to the most significant degradation rate, as indicated in [26]. The cyclic load frequency is set at 4 Hz, consistent across all temperature conditions and applied load levels. During various fatigue experiments, the temperature within the SRR piece during testing is closely monitored, ensuring that the maximum increase remains below the 10 °C limit as specified in [26].
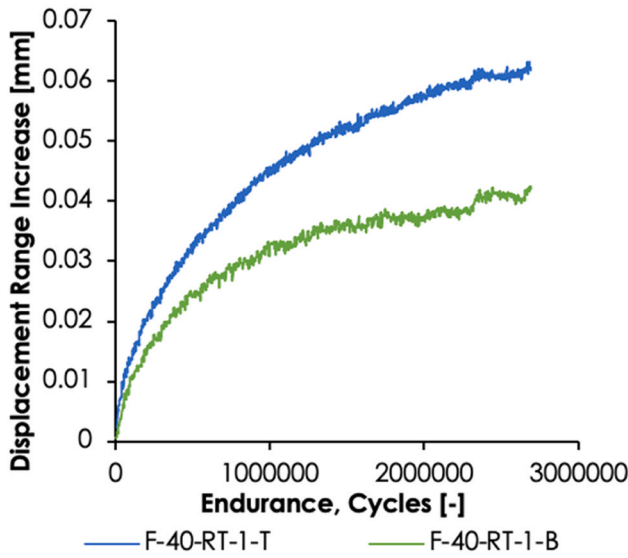
Throughout the cyclic tests, the range (max-to-min) of the connector's shear displacement is recorded while maintaining a constant load range. The connector displacement is defined as the local differential displacement of the steel plate and the composite bottom facing close to the connector, as shown in Fig. 5 **(c)**. For the sake of maintaining structurally and functionally reliable performance of hybrid bridge structures under cyclic loading a serviceability failure criterion under long-term loading is considered in this study. The force versus number of cycles (F-N) curves are defined not as an actual failure but as an increase of the displacement range due to cyclic loading. In case of slip-resistant connectors, a slip range increase of 0.3 mm has been frequently adopted as a failure criterion [24]. This threshold is based on the assumption that connectors with a slip range increase beyond 0.3 mm may no longer provide the desired level of resistance against slip under long-term loading, potentially compromising the structural integrity and performance of the overall system.

For practical reasons and based on observations from early testing phases, the test durations are tailored to optimize data collection while ensuring efficiency. At ± 60 kN load level and 25 °C, reaching the 0.3 mm displacement increase criterion around 1.5 million cycles set a baseline for consistent termination across subsequent tests. In contrast, at ± 40 kN level, where no significant displacement trend is observed up to 1.5 million cycles, the tests are extended to 2.5 million cycles. This allowed for a more comprehensive data set, providing valuable insights into the post-cyclic behaviour of the connectors. Similar approach is adopted for the connectors tested at higher temperature. Table 5 presents a detailed summary of the adopted termination criteria for the cyclic experiments, which takes into account both the specific load levels and the temperatures applied.
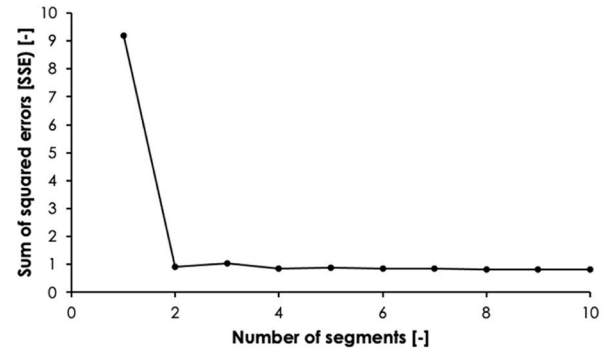
The specimens are installed and instrumented before preloading the bolts. A torque level of 900 Nmm is applied for experiments tested at the low and medium load levels, while a torque of 1350 Nmm is employed for the highest load level. Since all the specimens were stored in laboratory conditions, the cyclic tests at ambient temperature commence immediately once the bolts are preloaded. For the elevated temperature tests, insulation plates are then placed around the specimen, and the chamber is sealed. The interior temperature is increased to the target value at a rate of 0.1 °C/min Once the target temperature is achieved, it is precisely maintained within a 0.2 °C variance throughout the duration of both cyclic and static tests. To ensure uniform and stable temperature conditions within the connectors, specimens are held at the elevated temperature for a 24-hour period before commencing the cyclic tests. Subsequently, the cyclic test proceeds until reaching a predefined number of cycles, as detailed in Table 5.

3.2. Defining a failure criterion

As previously noted, for iSRR connectors embedded in fibre-polymer composite deck panels and tested under low load levels, the attainment of the limit of 0.3 mm displacement range increase through direct testing is considered impractical. Consequently, the specimens were subjected to testing only up to a certain number of loading cycles. This approach precludes the possibility of constructing a conventional F-N curve. As a viable alternative, the 0.3 mm failure criterion is estimated

(a) Recorded connectors' displacement range increase

(b) Recorded connectors' displacement range increase and their projection in log-log axis

Fig. 9. Displacement range increase of iSRR connector under loading cycles of ± 40 kN and room temperature.

(a) Elbow method to determine optimal number of segments

(b) Segmented linear regression with projections to 0.3 mm increase

Fig. 10. Estimating failure based on displacement range increase of iSRR connector.

are detailed below.

3.3.1. Linear regression analysis

This method, aimed at estimating the cycle count necessary to reach the 0.3 mm displacement threshold, employs selective linear regression analysis on a carefully chosen subset of the total displacement range data. The selection of data points is a critical step, designed to ensure a satisfactory c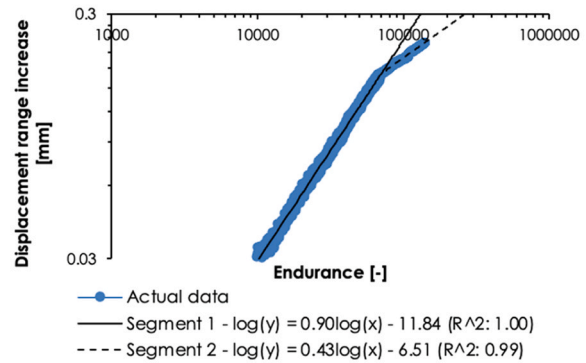oefficient of determination (R^2). In the present study, the threshold for the coefficient of determination of 0.97 was chosen, assuming that such a high R^2 value leads to a robust and statistically significant fit. Specifically, data points contributing to significant deviations, especially those in the later stages of the dataset, are excluded to enhance the accuracy of the model. Excluding the sub-set of data attributed to late cycles always leads to conservative results in this study because the second stage of cyclic behavior shows a lower stiffness degradation rate.

The analysis proceeds by plotting the refined dataset on a log-log scale, followed by the fitting of a trendline. This fitted model is then used for extrapolation to estimate the number of cycles required to reach the displacement range increase limit. Such a methodical selection and analysis of data points strike a balance between the precision of the trendline fitting and the representativeness of the dataset. The ultimate aim is to construct a model that reliably predicts the cycle count while maintaining the integrity and statistical significance of the data analysis.

For instance, an examination of two connectors tested on the same specimen under ± 40 kN load cycles until 2.5 million cycles revealed maximum range increases of 0.04 and 0.06 mm, as illustrated in Fig. 9 (a). When this data is plotted on logarithmic axes, a power law trendline can be fitted to estimate the number of load cycles that would result in a

by extrapolation of the log-log correlated test results towards the point at which this limit would be attained.

3.3. Displacement range increase extrapolation methods

In this section, two distinct methodologies are delineated for estimating the number of cycles required to reach the 0.3 mm displacement range increase threshold. The initial method involves executing linear regression analysis in log-log scale on the complete dataset of displacement ranges. In contrast, the subsequent approach commences with the segmentation of data into distinct groups, each characterized by their unique trendlines. This is followed by performing separate linear regression analyses on each individual segment. These methodologies
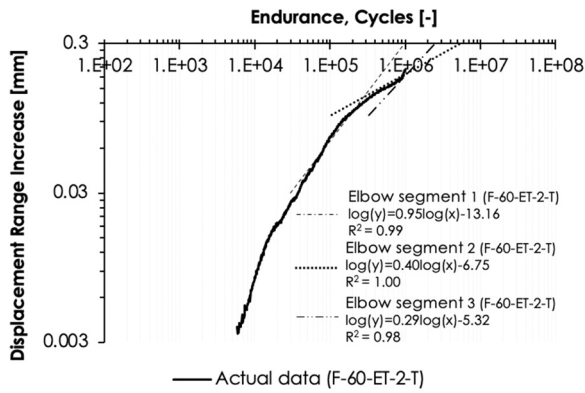
Fig. 11. Projecting all slopes of displacement range increases of iSRR connector tested at ± 60 kN and elevated temperature.

maximum slip limit of 0.3 mm. Fig. 9(b) indicates that this threshold is projected to be reached after 70 to 200 million cycles for the top and bottom connectors, respectively. Results for all specimens, including discussion are shown in Section 4.

3.3.2. The Elbow method

In this approach, prior to the linear regression analysis, a combination of 'change point analysis' and subsequent model fitting is implemented. The elbow method is integrated with linear regression for precise data segmentation, optimizing the fitting process. Breakpoints within the dataset are selected to minimise the sum of squared errors (SSE) for each data segment. The SSE for each cluster is computed by summing the squared distances from each data point to the centroid, which is the average of all data points within the cluster.

The selection of these breakpoints establishes the start and end points of each linear segment. This process entails iteratively adjusting breakpoints for varying numbers of segments, fitting individual linear models to each segment, and computing the SSE for each model. The optimal number of segments is determined at the point where a noticeable 'elbow' appears in the plot of SSE against the number of segments, as depicted in Fig. 10 (a). This point represents an equilibrium between model simplicity and accuracy. It's important to note that the segmentation is not merely an even division of the data range. Instead, it reflects the most statistically efficient division points within the dataset, as influenced by the natural clustering of data points. This approach ensures that each segment accurately represents a distinct pattern in the data, rather than a uniform or arbitrary division.

After segmenting the displacement range data, linear regression analysis is applied to each segment. The resulting trendlines provide the basis for extrapolating the estimated number of cycles needed for the displacement range to reach the specified 0.3 mm threshold. This extrapolation process, as depicted in Fig. 10 (b), predicts when the displacement threshold is likely to be met for each segment.

For many connectors, it is observed that the displacement range increase exhibits more than one distinct slope. The specimens initially display a certain slope that decelerates during the second stage, which then sometimes even rapidly increases (third stage) after several cycles to reach the failure criterion. The slip increase of the connectors demonstrates a fast-slow-fast trend, which mirrors the three-stage stiffness degradation trend commonly observed in composite materials [39]. This acceleration could potentially be attributed to several factors, such as the coalescence of cracks within the SRR piece, debonding between the SRR piece and the embedded nuts or the composite facing, or elongation of the hole in the bottom composite facing. However, it is important to note that these potential causes are hypothetical, and further investigation would be needed to conclusively identify the underlying mechanisms responsible for the observed acceleration.

The specimens that entered the third stage under cyclic loading were
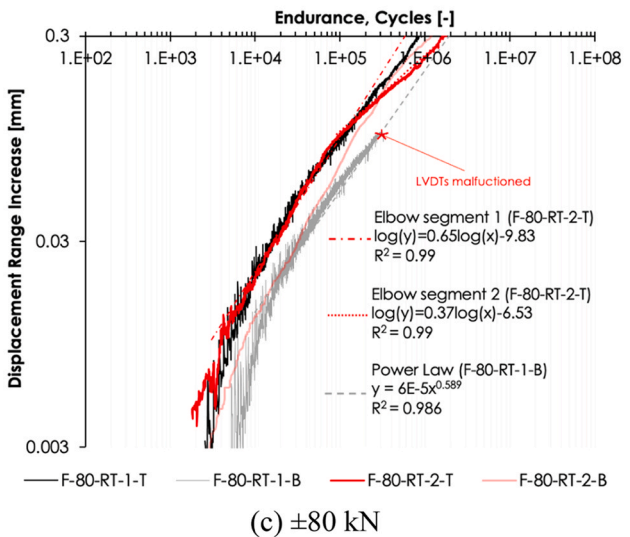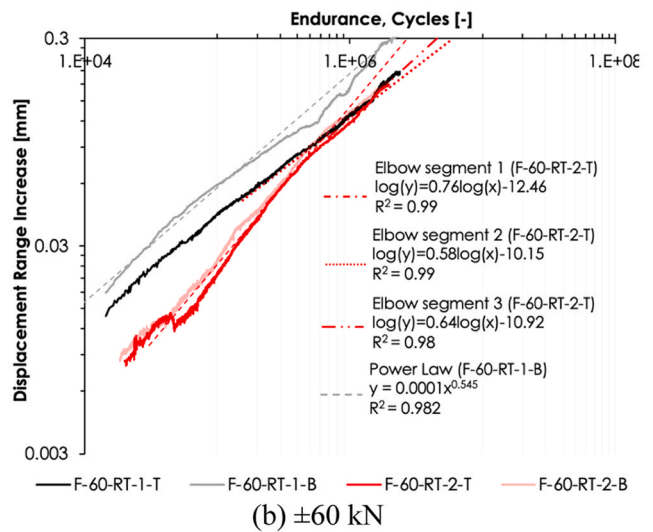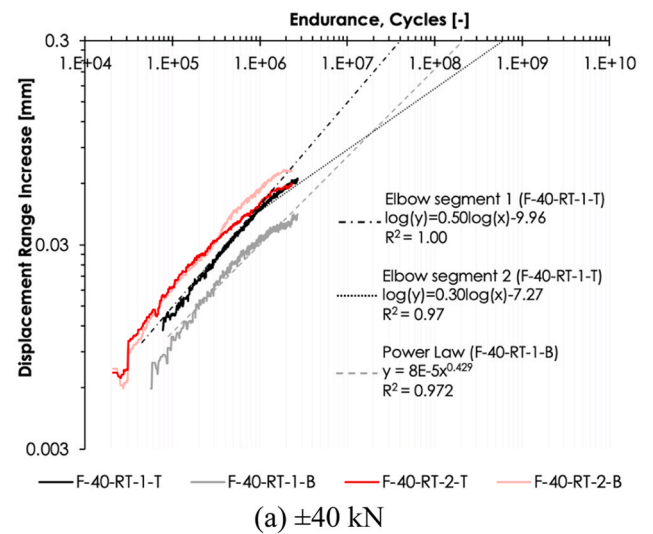

(a) ±40 kN

(b) ±60 kN

(c) ±80 kN

Fig. 12. Recorded connectors' displacement range increase in logarithmic scale axes under room temperature.

Table 6
Estimation of cycle counts until failure criterion at room temperatures.

Connector's ID	Parameter	Linear regression $y = A \cdot x^B$	Elbow method $\log(y) = A + B \cdot \log(x)$		
			Segment 1	Segment 2	Segment 3
F-40-RT-1-T	A	9E-5	-9.96	-7.27	-
	B	0.446	0.50	0.30	-
	R^2	0.984	1.00	0.97	-
	Cycles at 0.3 mm	79219349	45706665	464326422	-
F-40-RT-1-B	A	8E-5	-9.98	-6.69	-
	B	0.429	0.46	0.24	-
	R^2	0.972	0.98	0.81	-
	Cycles at 0.3 mm	200542936	130458047	12317402505	-
F-40-RT-2-T	A	0.0003	-9.82	-5.41	-
	B	0.369	0.50	0.19	-
	R^2	0. 976	0.99	0.84	-
	Cycles at 0.3 mm	133560224	26179036	5002122719	-
F-40-RT-2-B	A	0.0001	-8.00	-4.80	-
	B	0.450	0.36	0.13	-
	R^2	0.971	0.99	0.84	-
	Cycles at 0.3 mm	53536947	168402412	444482422162	-
F-60-RT-1-T	A	0.0001	-9.43	-8.85	-10.10
	B	0.505	0.54	0.49	0.58
	R^2	0.995	0.98	0.99	0.94
	Cycles at 0.3 mm	7632430	4224924	5759815	4389254
F-60-RT-1-B	A	0.0001	-9.02	-7.07	-10.33
	B	0.545	0.53	0.37	0.62
	R^2	0.982	0.98	0.97	0.92
	Cycles at 0.3 mm	2425074	2249997	2316044	6343799
F-60-RT-2-T	A	1E-5	-12.46	-10.15	-10.92
	B	0.677	0.76	0.58	0.64
	R^2	0.996	0.99	0.99	0.98
	Cycles at 0.3 mm	4131516	2813311	4945146	6343799
F-60-RT-2-B	A	2E-5	-12.25	-8.76	-9.20
	B	0.653	0.75	0.49	0.52
	R^2	0.988	1.00	1.00	0.99
	Cycles at 0.3 mm	2478906	2539788	5348033	4870016
F-80-RT-1-T	A	0.0002	-9.42	-8.57	-
	B	0.540	0.61	0.54	-
	R^2	0.989	0.99	0.96	-
	Cycles at 0.3 mm	765296	704712	871843	-
F-80-RT-1-B	A	6E-5	-13.07	-7.81	-
	B	0.589	0.86	0.40	-
	R^2	0.986	0.99	0.96	-
	Cycles at 0.3 mm	1772061	922742	13421785	-
F-80-RT-2-T	A	0.0004	-9.83	-6.53	-
	B	0.469	0.65	0.37	-
	R^2	0.978	0.99	0.99	-
	Cycles at 0.3 mm	1349567	600045	1932736	-
F-80-RT-2-B	A	0.00013	-11.07	-7.85	-6.30
	B	0.553	0.73	0.48	0.36
	R^2	0.987	1.00	0.67	0.52
	Cycles at 0.3 mm	1191821	743953	1099045	1255040

Table 7
Cycles at intersection between stage 1 and stage 2 based on elbow approach.

Max force [kN]	End of 1st stage [Cycles]
40	1606826
60	338831
80	200995

carefully examined to determine the most appropriate approach for constructing the F-N curve. It was ascertained that extrapolating the initial slope of the displacement range increase in a log-log scale to reach the slip limit offered the most conservative assumption. The conservative nature of this approach is demonstrated in Fig. 11, where the initial slope precedes the third stage, which accounts for the rapid increase in the displacement range. Alternatively, projecting the slope of the second stage could potentially lead to an overestimation of the number of cycles required to reach failure. Even when the displacement range of 0.3 mm

Table 8
Confidence bands of iSRR connector at room temperature conditions based on ASTM E739.

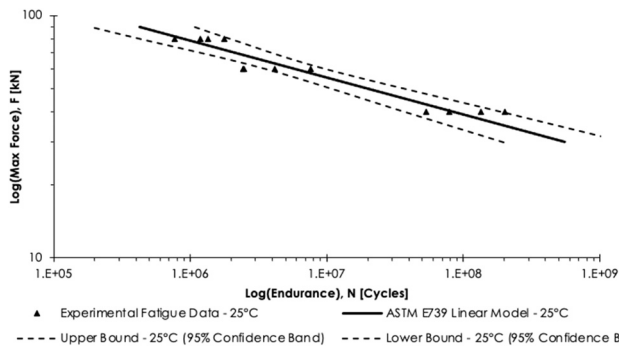|		Average		Lower bound		Upper bound	
		Linear	Elbow	Linear	Elbow	Linear	Elbow
Model parameters	A	18.4	18.5	16.0	16.2	18.5	20.8
	B (slope)	-6.5	-6.7	-7.9	-8.0	-6.7	-5.4
Cycles at specified max Force	40 kN	84577702	61801392	37457100	26179000	190983000	135446000
	60 kN	5998346	4093158	3622820	2518210	9931970	6653150
	80 kN	917580	596468	428621	286499	1964420	1241810

Fig. 13. Preliminary F-N curve (R = −1) for iSRR connector at room temperature with statistical analysis based on ASTM (data collected using elbow method).

Table 9
Average confidence bands of iSRR connector at room temperature conditions.

		Average	Lower bound	Upper bound
Model parameters	A	18.45	16.1	19.65
	B (slope)	-6.6	-7.95	-6.05
Cycles at specified max Force	40 kN	73189547	31818050	163214500
	60 kN	5045752	3070515	8292560
	80 kN	757024	357560	1603115

is reached by a connector, the cycles obtained from extrapolating the first stage slope are employed in the construction of the F-N curve. This was done to ensure uniformity in the analysis approach and a consistent conservative nature of all relevant data.

3.4. Post-cyclic static experiments

Once the cyclic test meets the stop criterion, the joint specimens are prepared for loading until their ultimate limit state under displacement-controlled loading at a constant rate of 0.01 mm/sec. Static experiments that do not utilize LVDTs but employed 3D DIC are not performed immediately after the completion of their respective cyclic tests. Specifically, these decks are dismantled after the cyclic loading, painted with a speckled pattern, and preloaded again to the steel end detail that is clamped to the machine. Then, the monotonic loading is applied, and the displacement of each connector is determined as an average measurement between the two DIC systems. In contrast, static tests employing LVDTs are executed immediately upon the completion of the cyclic test, thereby obviating the necessity for supplementary preloading. Some tests are manually terminated when at least 6 mm displacement increase is exceeded due to lack of further piston displacement.

4. Results and discussion

4.1. Cyclic tests at room temperatures

Fig. 12 presents the displacement range increase curves for various connectors, plotted in log-log scale for clarity of trend analysis. Among all, four connectors achieve the 0.3 mm displacement range increase threshold, highlighting the variability in their behaviour under cyclic loading conditions. In contrast, the remaining specimens are halted at pre-established cycle counts, not reaching this threshold. Additionally, the figure serves as a comparison between the linear regression and elbow segmentation methods, illustrating the process of extrapolating the number of loading cycles required to reach the failure criterion using these two distinct approaches. For further insights, Table 6 provides more comprehensive details related to this analysis.
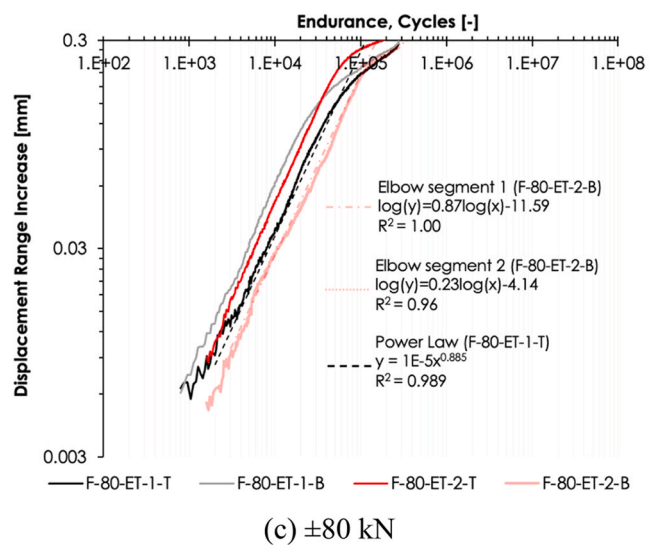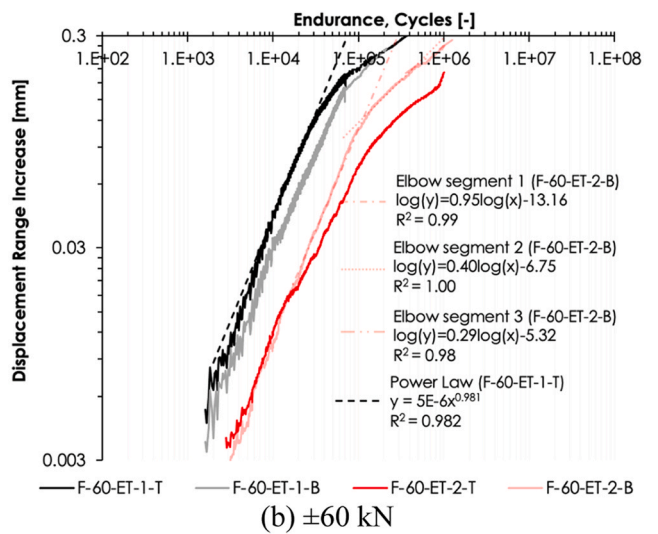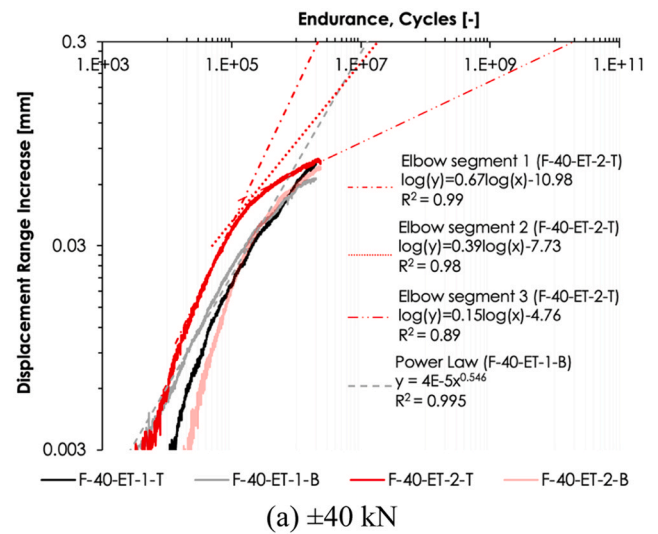

Fig. 14. Recorded connectors' displacement range increase and their projection in logarithmic scale axes at 55 °C.

Table 10

Cycles at intersection between stage 1 and stage 2 based on elbow approach.

Max force [kN]	End of 1st stage [Cycles]
40	181941
60	125047
80	72020

All connectors transition into the second stage, characterized by a lower displacement range increase rate, with five of them progressing to a third stage as identified by the elbow method. The number of cycles necessary for entering the second stage varies among the tested load levels, as detailed in Table 7. On average, a total of 1.6 million cycles is required for the connectors to enter the second stage of displacement range increase when subjected to a maximum load of 40 kN. The required cycles decrease by factors of 4.7 and 8 when the iSRR connectors are tested under ± 60 kN and ± 80 kN load conditions,

Table 11

Estimation of cycle counts until failure criterion at elevated temperatures.

Connector's ID	Parameter	Linear regression $y = A \cdot x^B$	Elbow method $\log(y) = A + B \cdot \log(x)$ Segment 1	Segment 2	Segment 3
F-40-ET-1-T	**A**	3E-5	-10.74	-7.27	-
	B	0.555	0.59	0.30	-
	R²	0.987	1.00	0.97	-
	Cycles at 0.3 mm	16259422	10400394	146991590	-
F-40-ET-1-B	**A**	4E-5	-9.99	-6.65	-
	B	0.546	0.54	0.34	-
	R²	0.995	0.99	0.98	-
	Cycles at 0.3 mm	12582950	11671145	594549559	-
F-40-ET-2-T	**A**	3E-5	-10.98	-7.73	-4.76
	B	0.625	0.67	0.39	0.15
	R²	0. 988	0.99	0.98	0.89
	Cycles at 0.3 mm	2498895	2377201	22768569	16106907285
F-40-ET-2-B	**A**	3E-06	-14.95	-10.88	-8.96
	B	0.762	0.95	0.61	0.45
	R²	0.982	0.99	0.97	0.93
	Cycles at 0.3 mm	3659338	1880194	8257362	27314990
F-60-ET-1-T	**A**	5E-6	-13.18	-8.82	-6.81
	B	0.981	1.08	0.65	0.46
	R²	0.982	0.99	0.96	0.79
	Cycles at 0.3 mm	74080	64664	126910	185147
F-60-ET-1-B	**A**	4E-6	-11.84	-6.51	-
	B	0.946	0.90	0.43	-
	R²	0.994	1.00	0.99	-
	Cycles at 0.3 mm	122798	130975	262740	-
F-60-ET-2-T	**A**	1E-5	-10.30	-5.54	-9.16
	B	0.772	0.66	0.28	0.54
	R²	0.998	0.98	0.99	0.90
	Cycles at 0.3 mm	627882	1006509	6447920	2247600
F-60-ET-2-B	**A**	1E-6	-13.16	-6.75	-5.32
	B	0.990	0.95	0.40	0.29
	R²	0.995	0.99	1.00	0.98
	Cycles at 0.3 mm	339882	296316	1009745	1697982
F-80-ET-1-T	**A**	1E-5	-7.92	-4.58	-
	B	0.885	0.56	0.27	-
	R²	0.989	0.99	1.00	-
	Cycles at 0.3 mm	114674	150465	249337	-
F-80-ET-1-B	**A**	3E-5	-7.62	-3.31	-
	B	0.807	0.57	0.13	-
	R²	0.976	1.00	0.55	-
	Cycles at 0.3 mm	90496	82689	320917	-
F-80-ET-2-T	**A**	1E-05	-11.23	-4.56	-
	B	0.894	0.89	0.28	-
	R²	0.996	1.00	0.97	-
	Cycles at 0.3 mm	101327	74894	141304	-
F-80-ET-2-B	**A**	1E-05	-11.59	-4.14	-
	B	0.827	0.87	0.23	-
	R²	0.997	1.00	0.96	-
	Cycles at 0.3 mm	259233	164108	1099045	-

Table 12

Confidence bands of iSRR connector under elevated temperature based on ASTM E739.

		Average		Lower bound		Upper bound	
		Linear	Elbow	Linear	Elbow	Linear	Elbow
Model parameters	**A**	16.1	15.7	12.2	14.9	20.0	24.1
	B (slope)	-5.9	-5.7	-8.1	-10.1	-3.7	-4.8
Cycles at specified max force	**40 kN**	4808517	4023390	1295760	1113000	17845200	14544000
	60 kN	446338	403336	198198	182032	1005200	893678
	80 kN	82642	78871	24265	23733	281477	262112

Table 13
Average confidence bands of iSRR connector tested at elevated temperature.

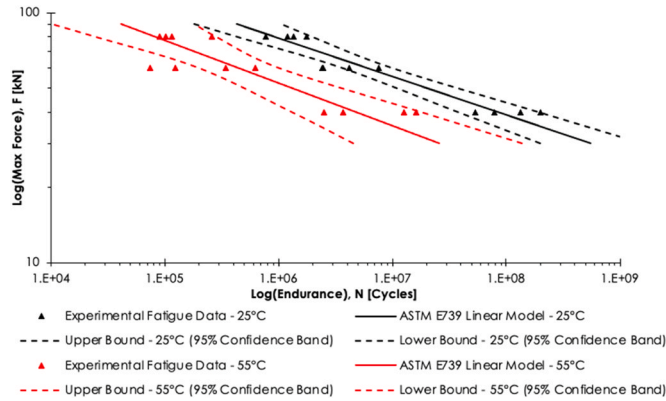|		Average	Lower bound	Upper bound
Model parameters	**A**	15.9	13.5	22.0
	B (slope)	-5.8	-9.1	-4.3
Cycles at specified max force	**40 kN**	4415954	1204380	16194600
	60 kN	424837	190115	949439
	80 kN	80757	23999	271795

Fig. 15. Preliminary F-N curve (R = −1) for iSRR connector under elevated temperature with statistical analysis based on ASTM E739 (data collected using elbow method).

respectively. This trend highlights the influence of loading conditions on the connectors' performance and their transition between different regimes of displacement range increase.

4.2. Fatigue life and F-N curve at room temperature

The extrapolated number of cycles to reach the 0.3 mm displacement range increase is used to construct the F-N data using both the linear regression and the Elbow method. The F-N relationship can be approximated by a straight line on a log-log scale, in accordance with the specifications of ASTM E739 [40]. The linear process is expressed by Eq. 1, where A and B represent the model parameters that are defined after performing linear regression. By substituting $\log(N) = Y$ and $\log(F_{max}) = X$, the relationship can be rewritten as Eq. 2.

$$\log(N) = A + B \cdot \log(F_{max}) \tag{1}$$

$$Y = A + B \cdot X \tag{2}$$

The 95 % confidence bands around the linear F-N curve are established, taking into account variations in data points, the number of tested specimens, and the force levels applied. To compute the Fp factor for the latter two parameters, the method outlined in [40] is employed. Table 8 details the cycle counts corresponding to the upper and lower 95 % confidence bands. Employing the 12 valid data points derived from the elbow method, regression parameters A and B are calculated to be + 18.5 and − 6.7, respectively, with B representing the F-N curve's slope which is commonly referred to as m. Fig. 13 illustrates the F-N curve based on the described statistical evaluation. A parallel analysis using linear regression without data segmentation yields closely aligned results: A at 18.4 and B at − 6.5 (m = −6.5). Table 9 presents the average results obtained from these two analytical approaches. Notably, the average slope of − 6.6 from this study is less steep than those reported in previous research: − 5.5 for pin-bearing failure of composite laminates with M16 bolted connections in a double-lap shear configuration as per [25], and − 4.4 for M20 Lindapter blind-bolted
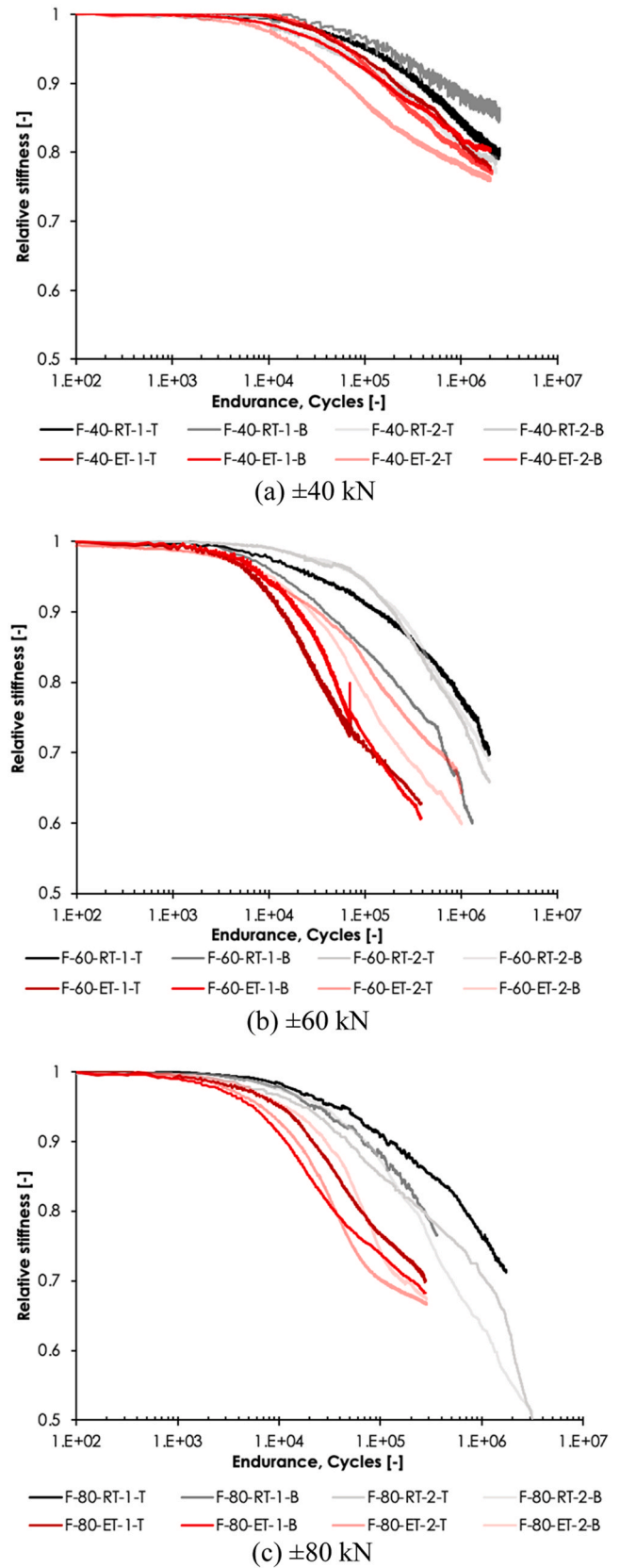

(a) ±40 kN

(b) ±60 kN

(c) ±80 kN

Fig. 16. Relative stiffness of iSRR connector at different cyclic load levels at room and elevated temperature.

(a) At room temperature
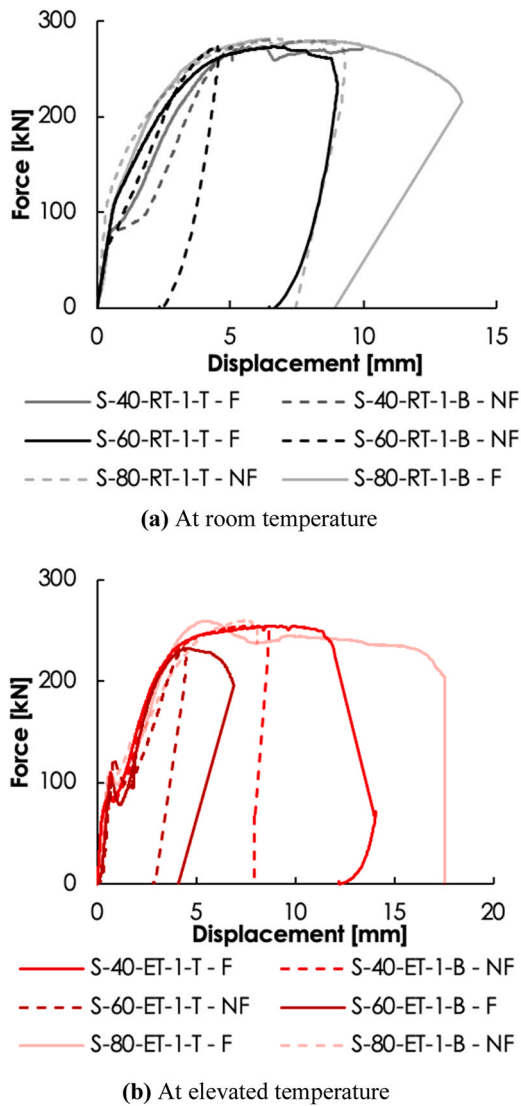

(b) At elevated temperature

Fig. 17. Representative force slip curves of iSRR connectors under post-fatigue short-term loading.

connections in a single-lap shear configuration according to [29].

4.3. Cyclic tests at elevated temperatures

Fig. 14 displays the displacement range increase for all tests conducted at elevated temperatures, represented in the log-log scale. The graph distinctly shows a linear trend in displacement range increase across all load levels until a nonlinear trend emerges in the second stage. Table 10 lists the varying cycles required for this transition. Similar to the room temperature tests, iSRR connectors under lower load levels necessitate more cycles to reach this nonlinear stage. Notably, all connectors exhibit a discernible second stage, with the elbow method indicating that five specimens commenced to a third stage. On average, at elevated temperature, the iSRR connector requires 182000 cycles to enter the second displacement stage under a fully reversed load of $\pm$ 40 kN. This cycle count decreases by factors of 1.4 and 2.5 under load conditions of $\pm$ 60 kN and $\pm$ 80 kN, respectively. When these findings are compared to those in Table 7 for room temperature conditions, the impact of temperature on connector performance and the transition between displacement stages becomes apparent.

Alike to the experiments done at room temperature, the two methods for projecting the curve following their trendline are applied to obtain

the cycles at which the serviceability failure criterion is reached. The cycles at which the projected lines reached the 0.3 mm of displacement range increase are reported in Table 11 and are used as an input to perform the statistical evaluation that generated the F-N curve of the iSRR connectors at 55 °C.

4.4. Fatigue life and F-N curve at elevated temperature

Consistent with the prior analysis, the statistical examination reveals that the F-N curve's slope at elevated temperatures is significantly steeper than that derived at room temperature, despite identical configurations, geometries, and load levels being considered. The 12 data points identified by the elbow method resulted in model parameters equal to B= −5.7 and A= +15.7, while the linear regression method yields slightly different estimates of B= −5.9 and A= +16.1. These values, along with the cycle counts for the 95 % confidence intervals pertaining to the iSRR connectors at elevated temperatures, are compiled in Table 12 for both analytical methods. Additionally, Table 13 provides the average outcomes from these two approaches. Illustrating these findings, Fig. 15 depicts the data points predicted by the elbow method and the resulted F-N curve and confidence bands delineated by red lines for the elevated testing temperatures. For comparative purposes, the F-N curve at room temperature is concurrently presented, providing a visual reference against the elevated temperature data.

4.5. Reflection on the credibility and accuracy of the prediction methods

The approach to extrapolate the displacement range increase until a certain threshold prioritizes conservative estimates to ensure safety and reliability in the predicted fatigue life of the iSRR connectors. Additionally, two distinct methods - linear regression analysis and the elbow method - were employed, and consistent results were observed across both, validating the approach. The methods were further validated by comparing their predictions against experimental data where the 0.3 mm displacement range increase was actually reached. In all cases, the predictions were found to be conservative, underscoring their credibility. In other words, the partial data set that was used to make prediction showed good validation when compared to the complete set of data. Although absolute accuracy is challenging in predictive modelling, the methodologies provide robust and credible lower-bound estimates, ensuring a reliable and conservative assessment of the connectors' fatigue life.

4.6. Stiffness degradation at different temperatures

The fatigue performance of connectors is also assessed by examining the relative stiffness under ambient and elevated temperatures. This metric is determined by dividing the load range per cycle by the respective displacement range. For comparability, stiffness values at each cycle were normalized to the initial stiffness from the first cycle. Fig. 16 reveals that, regardless of the applied load levels ($\pm$ 40, 60, and 80 kN), the connectors exhibit consistent stiffness, with values generally above 85 %. However, towards the conclusion of the tests, some cases depict a more significant drop, nearing 70 % of the initial stiffness.

Fig. 16 further dissects the effects of varying loads on relative stiffness at 25 °C. At a $\pm$ 40 kN load, the stiffness begins to decline around 10,000 cycles. However, with higher loads, this onset is earlier: 3500 cycles for $\pm$ 60 kN and 640 cycles for $\pm$ 80 kN. Comparing results from 25 °C to those at 55 °C shows differences in fatigue behavior. At 55 °C, the onset of stiffness decline emerges notably sooner, i.e., at 4400 cycles ($\pm$ 40 kN), 883 cycles ($\pm$ 60 kN), and 480 cycles ($\pm$ 80 kN). Moreover, the 55 °C stiffness curves consistently lie below the 25 °C curves throughout the tests, underscoring the compounded effects of elevated temperature and increased load.
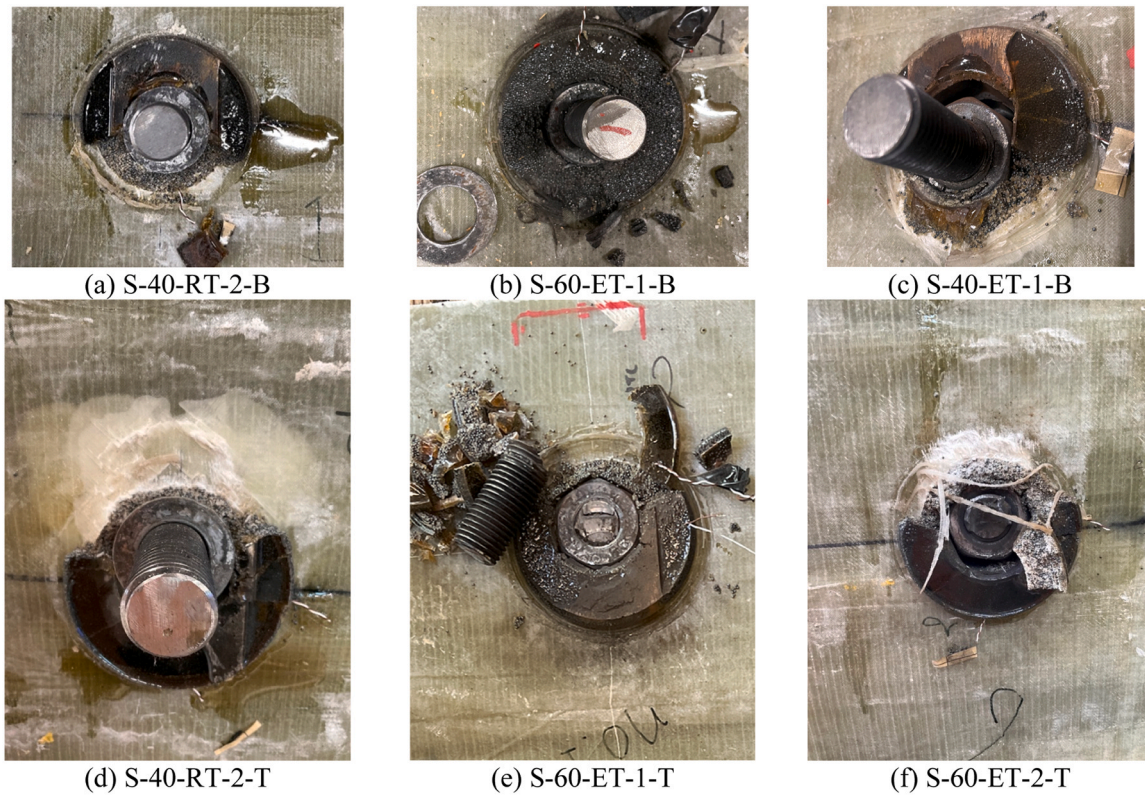
Fig. 18. Damages of composite deck and SRR piece with or without bolt shear failure of iSRR connectors.

Table 14
Post-cyclic static results from SLJ experiments under room temperature.

Connectors' ID	F_s [kN]	F_{ult} [kN]	δ_{ult} [mm]	$k_{sc,in}$ [kN/mm]
S-40-RT-1-T	84.5	273.5	5.22 *	183.0
S-40-RT-1-B	79.3		9.99 *	183.3
S-40-RT-2-T	70.5	241.2	18.13	346.0
S-40-RT-2-B	79.3		6.01 *	324.8
S-60-RT-1-T	112.7	273.5	9.02	163.1
S-60-RT-1-B	75.2		4.57 *	163.8
S-60-RT-2-T	77.9	282.1	5.39 *	265.7
S-60-RT-2-B	96.4		5.71 *	240.0
S-80-RT-1-T	106.9	281.4	13.71	178.6
S-80-RT-1-B	110.4		9.31 *	245.4
Average (COV)	-	270.4 (6.2 %)	-	229.4 (29.0 %)

Note: * - Non failed connector

Table 15
Post-fatigue static results from SLJ experiments under elevated temperature.

Connectors' ID	F_s [kN]	F_{ult} [kN]	δ_{ult} [mm]	$k_{sc,in}$ [kN/mm]
S-40-ET-1-T	84.8	254.9	9.3 *	325.2
S-40-ET-1-B	77.2		14.0	305.4
S-40-ET-2-T	78.2	267.7	16.8	257.6
S-40-ET-2-B	81.9		7.0 *	254.1
S-60-ET-1-T	109.7	232.9	6.9	231.3
S-60-ET-1-B	93.7		4.4 *	224.5
S-60-ET-2-T	98.5	240.4	15.4	264.2
S-60-ET-2-B	92.5		5.4 *	244.0
S-80-ET-1-T	104.7	259.8	8.1 *	170.4
S-80-ET-1-B	108.6		12.1	187.7
S-80-ET-2-T	118.0	273.4	6.0 *	179.9
S-80-ET-2-B	118.2		17.6	199.3
Average (COV)	-	254.9 (6.1 %)	-	236.9 (20.4 %)

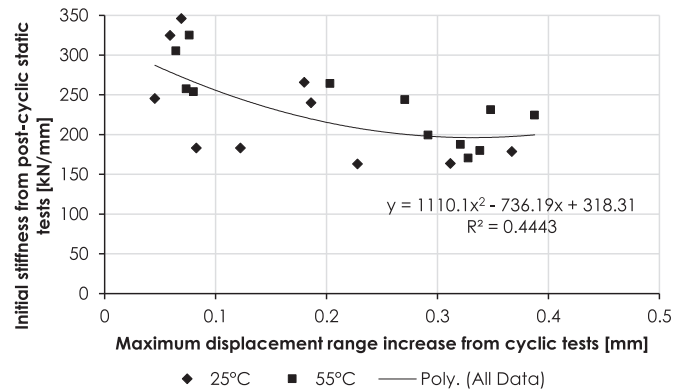Note: * - Non failed connector

Fig. 19. Correlation between initial stiffness of iSRR connector with the maximum displacement range increase from cyclic loading tests.

4.7. Post-cyclic static shear resistance at room and elevated temperature

The ultimate limit state static behaviour of the studied iSRR connectors is assessed by testing monotonically to the ultimate load of the specimens previously subjected to cyclic loading. This approach aligns with findings by Olivier et al. [26], who reported that iSRR connectors exposed to long-term loading prior to static tests exhibited similar ultimate forces and displacement at failure, relative to reference specimens subjected exclusively to static loading.

Representative force displacement curves are presented in Fig. 17. The displacement on the X-axis represents the relative slip between the steel plate and the bottom composite facing calculated based on average measurements from both sides of the connector. In cases where LVDTs are used, the 10 mm limit of the LVDTs is reached, necessitating readjustment during the testing period. Connectors that experienced failure are depicted with continuous lines, while non-failed specimens are

indicated by dashed patterns. Both static tests at room and elevated temperatures are conducted once the failure or stop criteria are met during cyclic loading.

The iSRR connectors experience a two-phase linear performance; initially displaying a steady increase in load until their slip resistance is surpassed, followed by a secondary linear trend until the maximum resistance is reached. At room temperature, the connectors achieved their peak load at an average slip of 6 mm, while at elevated temperatures, it is reduced to approximately 5 mm. Predominantly, the nut embedded closest to the steel stiffener detaches from the SRR piece, with the bolt shifting several millimetres towards the direction of the applied load, as illustrated in Fig. 18 **(c)**. Every test consistently exhibited bolt bending, with most of them presenting bolt shear failure, as depicted in Fig. 18 **(a, b, e, f)**. Under extreme scenarios where exceptionally high slip at failure is observed e.g., more than 16 mm, local crushing of the composite laminate along with indications of delamination became discernible, as shown in Fig. 18 **(d)**. However, these signs were absent in cases of failure at reduced slip levels. The simultaneous activation of these various dissipation mechanisms guaranteed significant ductility upon failure, with ultimate displacements exceeding 6 mm for all connectors. From the DIC results, no composite failure on both sides of the panel or out-of-motion performance is detected.

Table 14 and Table 15 summarize the static test results, highlighting initial stiffness ($k_{sc,in}$), slip resistance (F_s), ultimate load (F_{ult}) and slip at failure between the steel plate and composite deck (δ_{ult}). Variability in slip force can be primarily attributed to different torque levels during preloading. Specifically, connectors with a preload torque of 900 Nmm resulted in an average slip resistance of 87.0 ± 12.4 kN, while a torque of 1350 Nmm increases the slip force to 111.1 ± 5.7 kN. All the connectors display a low variation of their ultimate resistance, with a coefficient of variation being 6 % for both testing temperatures. Connectors tested under room temperature demonstrate a marginally higher average ultimate shear resistance compared to those tested at elevated temperature.

Notably, there is a pronounced variation in the $k_{sc,in}$ among the samples. This variability is largely attributed to the influences of the prior cyclic tests. To better comprehend the interplay between the cyclic tests and their impact on the resulting stiffness values, Fig. 19 is formulated. This representation correlates the maximum displacement range increase, derived from the fatigue experiments, with the initial stiffness acquired during the monotonic loading. A correlation emerges between these variables. The data integrated into this figure encompasses results from both tested temperatures. To depict this relationship, a 2nd order polynomial fitting function is chosen due to its highest R^2 value, consolidating data from both temperature tests. The observed correlation underscores the critical influence of cyclic loading on the connector's initial stiffness and highlights the importance of considering fatigue history in predicting their performance and durability in practical applications.

5. Concluding remarks

This study investigates the fatigue performance of iSRR connectors within glass fibre composite decks under room and elevated temperatures. Small segments of glass fibre composite sandwich web panels, measuring $600 \times 300 \times 200$ mm, were connected using preloaded M27 bolts to the steel plates that are used to impose shear loading to the connectors. The iSRR connector design ensures no loss of the bolt preloading. Fatigue performance of iSRR connectors was studied under fully reversed cyclic loading, with three load levels: low, medium, and high, equalling to ± 40, ± 60, and ± 80 kN respectively. Comparisons at the two distinct temperatures were made on the level of F-N curves, i. e. design fatigue life, and relative stiffness degradation graphs. Post cyclic static load was applied to determine the residual ultimate resistance of the iSRR connectors for hybrid steel-composite structures. From this, the following concluding remarks can be drawn:

1. The iSRR connectors demonstrated very good fatigue performance, with many tests not reaching the failure criterion, necessitating conservative extrapolation of damage to determine design life.
2. At an elevated temperature of 55 °C, the F-N curve showed a reduced slope to an average of 5.8 and a horizontal shift to the left.
3. Regardless of the temperature and the extent of damage from cyclic loading, the resistance of the iSRR connectors varied only by about 6 % around an average resistance value of 260 kN, indicating high resistance for such connectors in structural applications.
4. Post-cyclic static experiments yielded two distinct slip resistances with mean values of 87 kN and 111 kN corresponding to preload torques of 900 Nmm and 1350 Nmm, respectively. No reduction in preload or slip resistance was observed related to cyclic loading nor related to elevated temperatures, demonstrating that the iSRR connector retains its structural integrity and does not weaken under thermal stresses.

The iSRR connector proved to be a resilient solution for applications demanding consistent performance for serviceability limit state, ultimate limit state, ductility requirements and even in thermally challenging environments. Consequently, this study demonstrates the significant potential of iSRR joints in fatigue-dominated structures, such as composite-to-steel hybrid bridges.

CRediT authorship contribution statement

Marko Pavlovic: Writing – review & editing, Supervision, Project administration, Methodology, Funding acquisition, Conceptualization. **Angeliki Christoforidou:** Writing – original draft, Visualization, Validation, Software, Investigation, Data curation, Conceptualization.

Declaration of Competing Interest

The authors declare that they have no known competing financial interests or personal relationships that could have appeared to influence the work reported in this paper.

Data availability

Data will be made available on request.

Acknowledgements

References

[1] Snijder, H. and B. Hesselink. *Repair, strengthening and upgrading of steel bridges in The Netherlands*. in *IABSE Symposium Report*. 2017. International Association for Bridge and Structural Engineering.

[2] Institution BS. Eurocode 2: Design of concrete structures: Part 1-1: General rules and rules for buildings. British Standards Institution; 2004.

[3] Bakker J, et al. Leidraad RAMS: sturen op prestaties van systemen. Tilburg, Drukkerij Gianotten; 2010.

[4] De Larrard F, Sedran T. Optimization of ultra-high-performance concrete by the use of a packing model. Cem Concr Res 1994;24(6):997–1009.

[5] Duan M, et al. Experimental investigation of headed studs in steel-ultra-high performance concrete (UHPC) composite sections. Eng Struct 2022;270:114875.

[6] Marcos-Meson V, et al. Durability of Steel Fibre Reinforced Concrete (SFRC) exposed to acid attack–A literature review. Constr Build Mater 2019;200:490–501.

[7] Li, V.C., et al., Development of green engineered cementitious composites for sustainable infrastructure systems. 2004.

[8] Karbhari VM, Zhao L. Use of composites for 21st century civil infrastructure. Comput Methods Appl Mech Eng 2000;185(2-4):433–54.

[9] Sams, M., *Broadway bridge case study: Bridge deck application of fiber-reinforced polymer*. Transportation Research Record: Journal of the Transportation Research Board, 2005(CD 11-S).

[10] Fang H. Behavior of bolted shear connectors for demountable and reusable UHPC-formed composite beams. in Life-Cycle of Structures and Infrastructure Systems. CRC Press; 2023. p. 195–202.

[11] Pavlović M, et al. Bolted shear connectors vs. headed studs behaviour in push-out tests. J Constr Steel Res 2013;88:134–49.

[12] Milosavljević B, et al. Static behaviour of bolted shear connectors with mechanical coupler embedded in concrete. Steel Compos Struct Int J 2018;29(2):257–72.

[13] Kwon G, Engelhardt MD, Klingner RE. Behavior of post-installed shear connectors under static and fatigue loading. J Constr Steel Res 2010;66(4):532–41.

[14] Zhang Y, et al. Experimental and numerical analyses on the shear behavior of grouped single-embedded-nut high-strength bolts in steel–ultra-high-performance concrete composite slabs. J Build Eng 2024:108829.

[15] Marshall W, Nelson H, Banerjee H. An experiment study of the use of high-strength friction grip bolts as shear connectors in composite beams. Structural Engineer; 1971.

[16] Gresnigt AN, Stark JJ. Design of bolted connections with injection bolts. in Connections in steel structures III. Elsevier; 1996. p. 77–87.

[17] Ban H, et al. Time-dependent behaviour of composite beams with blind bolts under sustained loads. J Constr Steel Res 2015;112:196–207.

[18] Pathirana SW, et al. Flexural behaviour of composite steel–concrete beams utilising blind bolt shear connectors. Eng Struct 2016;114:181–94.

[19] Wang J-Y, et al. Push-out tests of demountable headed stud shear connectors in steel-UHPC composite structures. Compos Struct 2017;170:69–79.

[20] Vassilopoulos AP, Keller T. Fatigue of fiber-reinforced composites. Springer Science & Business Media; 2011.

[21] Park K-T, et al. Degree of composite action verification of bolted GFRP bridge deck-to-girder connection system. Compos Struct 2006;72(3):393–400.

[22] Smith P, Pascoe K. Fatigue of bolted joints in (0/90) CFRP laminates. Compos Sci Technol 1987;29(1):45–69.

[23] Heshmati M. Durability and long-term performance of adhesively bonded FRP/steel joints. Sweden: Chalmers Tekniska Hogskola; 2017.

[24] Moon F, Eckel D, Gillespie Jr J. Shear stud connections for the development of composite action between steel girders and fiber-reinforced polymer bridge decks. J Struct Eng 2002;128(6):762–70.

[25] van Wingerde AM, van Delft DRV, Knudsen ES. Fatigue behaviour of bolted connections in pultruded FRP profiles. Plast, Rubber Compos 2013;32(2):71–6.

[26] Olivier G, et al. Conventional vs. reinforced resin injected connectors' behaviour in static, fatigue and creep experiments on slip-resistant steel-FRP joints. Eng Struct 2021;236.

[27] Nijgh, M.P., New Materials for Injected Bolted Connections - A Feasibility Study for Demountable Connections. 2017, Delft University of Technology.

[28] Csillag F, Pavlović M. Push-out behaviour of demountable injected vs. blind-bolted connectors in FRP decks. Compos Struct 2021;270.

[29] Olivier G, et al. Static, fatigue and creep performance of blind-bolted connectors in shear experiments on steel-FRP joints. Eng Struct 2021;230.

[30] Xue C, et al. Experimental and numerical study on tensile properties of bolted GFRP joints at high and low temperatures. Compos Struct 2022;293:115743.

[31] Turvey G, Wang P. Failure of pultruded GRP single-bolt tension joints under hot–wet conditions. Compos Struct 2007;77(4):514–20.

[32] Wu C, Bai Y, Toby Mottram J. Effect of elevated temperatures on the mechanical performance of pultruded FRP joints with a single ordinary or blind bolt. J Compos Constr 2016;20(2):04015045.

[33] Liu L, et al. Tension-tension fatigue behavior of ductile adhesively-bonded FRP joints. Compos Struct 2021;268:113925.

[34] Ashcroft I, et al. Effect of temperature on the quasi-static strength and fatigue resistance of bonded composite double lap joints. J Adhes 2001;75(1):61–88.

[35] Christoforidou, A., et al. Fatigue performance of injected steel reinforced resin connectors in GFRP sandwich web core panels in 11th International Conference on Fiber-Reinforced Polymer (FRP) Composites in Civil Engineering (CICE 2023). 2023. Rio de Janeiro, Brazil: Zenodo.

[36] Olivier G, et al. Feasibility of bolted connectors in hybrid FRP-steel structures. Constr Build Mater 2023;383:131100.

[37] Christoforidou A, Verleg R, Pavlović M. Static, fatigue and hygroscopic performance of steel-reinforced resins under various temperatures. Submitt Publ 2023.

[38] Gribnau, K., Shear force in bolted connections for hybrid steel-FRP bridges. 2021, Delft University of Technology.

[39] Gao J, et al. Strength and stiffness degradation modeling and fatigue life prediction of composite materials based on a unified fatigue damage model. Eng Fail Anal 2022;137:106290.

[40] ASTM. E739 10 standard practice for statistical analysis of linear or linearized stress-life. Annual Book of ASTM Standards; 1980.